FWI for model updates in large-contrast media

Sverre Brandsberg-Dahl, Nizar Chemingui and Alejandro Valenciano. PGS.

Abstract

We describe a new robust solution for recovering the long-wavelength features of a velocity model in FWI. The method uses reflected and transmitted wave modes, i.e. the full wavefield, to recover high-resolution velocity models. Our new FWI gradient enables reliable velocity updates deeper than the maximum penetration depth of diving waves, and reduces the FWI dependency on recording ultra-long offsets.

We also discuss a new FWI regularization scheme that overcomes the limitations of the inversion in the presence of high contrast geobodies and cycle skipping. The implementation makes use of the split Bregman method making it efficient and accurate.

Results from applying the new FWI gradient to field data show that we can combine both transmitted and reflected energy in a global FWI scheme to obtain high-resolution velocity models without imprint of the reflectivity on the velocity updates.

Introduction

Full Waveform Inversion (FWI) is now well established as a velocity estimation tool in the seismic industry. First introduced in the early 1980's by Tarantola, we had to wait almost 30 years until the technology achieved widespread acceptance. As stated, FWI has in intuitive and simple objective; minimize data misfit. However, in practice, this is clearly a complex task that requires the use of forward modeling to generate data, optimization algorithms and regularization to help cope with the inherit non-linearity of the problem.

The delay in uptake can maybe firstly be attributed to the, at the time, lack of cost effective compute solutions powerful enough to solve the many forward modeling and imaging iterations needed as part of the FWI implementation. Seismic acquisition equipment and templates from this era also posed challenges; offsets were limited or even short, and recording systems were often equipped with harsh low-cut filters effectively eliminating the low frequencies needed for FWI. It is important to keep in mind that the goal at the time was to acquire data for reflection seismology; so little focus was put on the ability to record refractions and diving waves.

OBC and OBN data were used in some early applications FWI as they circumvent these issues by decoupling the sources and receivers, providing long offset, rich and even full azimuth coverage and more reliable recordings of the low frequencies. Lately, applications to streamer data have become more widespread as the availability of long offset data with good low frequency content has increased. This has help to truly establish FWI in the mainstream, in particular from a data volume perspective as 3D streamer seismic covers far more areas than nodes or OBC. Lately, use of multi vessel acquisition schemes that can acquire very long offsets have further progressed this, enabling streamer-based recording of the diving waves and refractions that are so important for achieving convergence in most FWI schemes.

FWI inverts for the velocity model by solving a nonlinear inverse problem minimizing the difference between modeled data and recorded field data (Tarantola, 1984). A schematic illustration is shown in Figure 1. The matching is quantified by the residuals of a least-squares objective function, and the model update is computed as a scaled representation of its gradient. For most, if not all exploration seismic applications, FWI is an ill-posed problem due to the band-limited nature of the seismic data and the limitations of the acquisition geometries; we do not have access to the full wavefield. To mitigate this, typical FWI implementations involve iterative solution schemes with various forms of regularization applied to gradients and/or solutions. It is also common to approach FWI with a multi-scale approach, i.e. starting from low frequencies and adding higher frequencies to the problem as the recovered model improves. Provided the right data, FWI can produce high-resolution models of the subsurface when compared to ray-based methods.
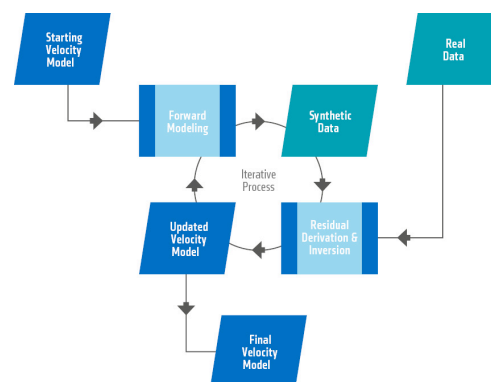

Figure 1. *Conceptualized overview of the Full waveform inversion scheme*

Method

In conventional FWI, we solve a nonlinear inverse problem by iteratively updating the model to minimize an objective function, which is the difference between the modeled seismic data and the recorded field data. This misfit function is generally minimized in a least-squares sense, and the model update is computed as a scaled representation of its gradient. In the case of an isotropic acoustic medium parameterized in terms of bulk-modulus and density (κ, ρ), Tarantola (1984) shows that the gradient depends on the kernels for κ and ρ that can be written as:

$$K_\kappa(\mathbf{x}) = \frac{1}{\kappa(\mathbf{x})} \int \frac{\partial S(\mathbf{x},t)}{\partial t} \frac{\partial R(\mathbf{x},T-t)}{\partial t} dt \quad \text{and} \quad (1)$$

$$K_\rho(\mathbf{x}) = \frac{1}{\rho(\mathbf{x})} \int \nabla S(\mathbf{x},t) \cdot \nabla R(\mathbf{x},T-t) dt, \quad (2)$$

where $\kappa(\mathbf{x}) = \rho(\mathbf{x})v^2(\mathbf{x})$ is the equation that relates the bulk-modulus to velocity, $S(\mathbf{x},t)$ is the source wavefield and $R(\mathbf{x},T-t)$ is the residual wavefield after time reversal. Equations (1) and (2) are sensitivity kernel for the respective parameter, and measures the variation in the misfit function caused by change in that parameter while holding the others fixed. The sensitivity kernels corresponding to Equations (1) and (2) for a simple tow-layer model are shown in Figures 1a and 1b. Note how the back-scattered energy in the kernels, or "rabbit ears", changes polarity in the two images. This is a fact that was recognized in the work of Whitmore and Crawley (2012), where they introduced a new RTM imaging condition formed by the summation of two kernel components to suppress low-wavenumber imaging artifacts. For the RTM application the aim was to remove the low wavenumbers, so quite opposite of what we aim to do for FWI. Using the sensitivity kernels in Equations (1) and (2), we can express new kernels in terms of bulk modulus and density by simply forming linear combinations

$$K_v(\mathbf{x}) = K_K(\mathbf{x}) - K_\rho(\mathbf{x}) \qquad (3)$$

$$K_Z(\mathbf{x}) = K_K(\mathbf{x}) + K_\rho(\mathbf{x}), \qquad (4)$$

where the impedance kernel in Equation (4) can be recognized as the RTM imaging condition presented by Whitmore and Crawley (2012). The impedance kernel comprises the high wavenumber components of the velocity field while removing the unwanted backscattered noise. The examples presented in their paper, using heterogeneous models, highlighted the importance of dynamically weighting the different components of the impedance kernel to achieve optimal removal of the low wavenumber artifacts. Figure 1c shows the result of weighting the components from Figures 1a and 1b, to produce an RTM impulse response free of back-scattered noise.
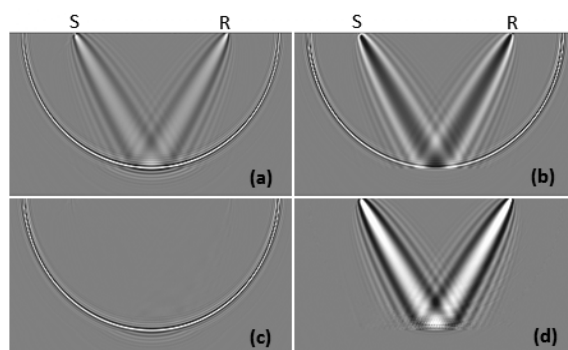

Figure 1. *Sensitivity kernels of a source-receiver pair in a model with a homogeneous layer overlying a half-space: (a) bulk-modulus, (b) density, (c) impedance, and (d) velocity*

On the other hand, the velocity kernel given by Equation (3) is ideal for FWI where the low wavenumber components of the gradient are preferred. As we know, the high wavenumbers associated with reflections may mislead the inversion. Following the premises of Whitmore and Crawley (2012), an FWI gradient can be derived by dynamically weighting the velocity sensitivity kernel (Equation 3). Their dynamic weights can be adapted to alternatively remove the high wavenumbers from the FWI gradient in a heterogeneous media. The new FWI gradient derived from equation (3) is:

$$G(\mathbf{x}) = \frac{1}{2A(\mathbf{x})} \left\{ \int_t \left[W_1(\mathbf{x},t) \frac{1}{v^2(\mathbf{x})} \frac{\partial S(\mathbf{x},t)}{\partial t} \frac{\partial R(\mathbf{x},T-t)}{\partial t} \right] dt - \int_t \left[W_2(\mathbf{x},t) \nabla S(\mathbf{x},t) \cdot \nabla R(\mathbf{x},T-t) \right] dt \right\} (5)$$

where the dynamic weights $W_1(\mathbf{x},t)$ and $W_2(\mathbf{x},t)$ are designed to optimally suppress the migration isochrones, and $A(\mathbf{x})$ is the illumination term. Figure 1d is produced using equation 5; it illustrates how the migration isochrone has been removed while the low wavenumber energy is preserved.
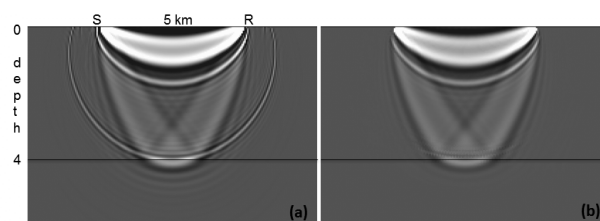

Figure 2. *Sensitivity kernels of a source-receiver pair in a model with a V(z) layer overlying a half-space: (a) conventional kernel and (b) dynamically weighted velocity kernel.*

Figure 2a shows the conventional FWI gradient compared to the modified gradient from Equation 5 (Figure 2b) in a simple v(z) velocity model where velocity is linearly increasing with depth. Here, the modified gradient in Equation 5 removes the migration operator (isochrone), but preserves all the low wavenumber components associated with the diving waves ("bananas") and backscattering ("rabbit ears"). To better illustrate the use of reflections in FWI we use a simple 2D synthetic example consisting of five homogeneous layers, as shown in Figure 3. The data has maximum offsets of 4 km so only pre-critical reflections are used in the inversion. The starting velocity model for FWI contained errors up to 100m/s. The inversion was performed on a frequency band of 3-5 Hz. Figures 3b and 3c, show the results of the inversion using the conventional FWI gradient as compared to our new FWI gradient. Results from the new FWI gradient are accurate and do not suffer from the high wavenumber artifacts observed on the conventional FWI update, that is dominated by the reflections as would be observed in a migrated image.
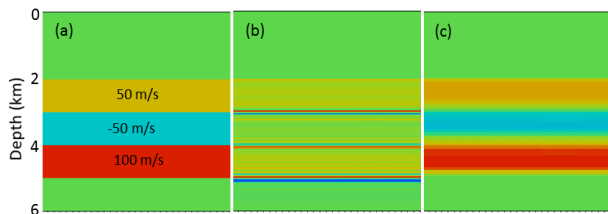

Figure 3. *Five layer synthetic model: (a) Difference between exact and starting model, and between the inverted and the initial velocity model using the (b) conventional and (c) new FWI gradients.*

Limitations to current implementations: shallow water, reflectivity

Although well established as part of the velocity model building flow, most successful applications of FWI to date have been limited to shallow water environments. This can be attributed to the fact that most implementations rely heavily on refracted energy or diving waves. Put this together with the offset limitations that exist in seismic data, stream and node alike, it follows naturally that shallow setting lend themselves easiest to being addressed by FWI as they are better sampled by refractions. A recent application of FWI to shallow water OBC was given by Liu et al. (2011) where accurate over burden velocities were obtained using refractions. This not only improved the shallow imaging, but also resolved depth ambiguities and miss-ties at reservoir level. A similar case using data from a dual-sensor towed streamer acquisition was presented by Zhou et al. (2014) where the authors show that modern streamer data contains refractions that produce good FWI velocity updates down to a depth of about 1/4 of the streamer length. In these scenarios, FWI relied mainly on recorded diving waves to resolve small-scale geologic features up to the deepest turning point. For deeper targets, FWI needs to rely on reflected energy to update the model. However, as we will see later, using the conventional FWI gradient computation in such situations is challenging

unless the recorded reflections have extraordinary low-frequency content.

Beyond the depth limitations of refractions, a range of factors will influence how well FWI will resolve the velocities in the sub-surface. A key role is actually played by the rock formations over which the seismic was acquired; harder rocks (well-consolidated) tend to have good correlation between velocity and reflectivity, which is a common assumption in most FWI implementations. A typical FWI scheme uses an explicit relationship between density and velocity in the forward modeling step, such as Gardner's relation, so there is an intrinsic assumption that change in reflectivity is also a change in velocity. However, in many softer rocks and unconsolidated sediments, the reflectivity is typically correlated to density changes and not velocity changes, as the latter is typically driven by changes in pressure, burial history etc. When applying FWI in basins with such characteristics, for example the Gulf of Mexico, great care must be take avoid that the FWI updates not only maps reflectivity into the velocity model. FWI might produce a "pretty" velocity field, but it is often an erroneous representation of what is actually happening in the subsurface.

To move beyond the typical limitations outlined above, there has been a furry of activity in the recent years to reformulate FWI algorithms to include reflected energy for retrieving long-wavelength updates (e.g., Xu et al., 2013; Zhou et al., 2015, Alkhalifah, 2015). The fundamental idea is to compute a gradient in which undesired reflectivity (migration isochrones) are not present, such that indeed the full wavefield can by used in FWI to produce high resolution velocity models that correctly predicts refractions and reflections, a key step when using the models for depth migration and imaging. These improvements to the physics of FWI are nicely complemented by the introduction of new and robust regularizations schemes to stabilize the solution to the inversion step of FWI, i.e. improving the mathematics of the implementation. FWI is particularly challenged when facing large contrast geobodies such as salt bodies or volcanics. In such situations, the FWI solution often gets trapped in local minima unless the starting model is very accurate. Introduction of Total Variation (TV) regularization (Guo and de Hoop, 2013) have offered important insights into how such situations can be mitigated when applying FWI to large scale field datasets.

In following pages, we will propose and review the concepts behind a new FWI gradient implementation that eliminates the migration isochrones that typically dominate FWI gradients in heterogeneous media. By separating the low from the high wavenumber components in the gradient, we can produce long wavelength velocity updates at depths greater than the penetration depth of the diving waves. Several data examples, both synthetic and field date, are used to highlight performance aspects of the method. Our new solutions are able to provide high resolution velocity models from records containing diving waves and reflections without the migration imprint provided by conventional FWI.

Results

To illustrate the impact of the new FWI gradient we use a field data from deep-water Gulf of Mexico (DeSoto Canyon). The data were acquired with dual-sensor streamers and with a maximum offset of 12 km. The FWI full-power frequency band was 3-7 Hz. No particular mutes or event selection were used, therefore all recorded data were employed during the inversion. Figure 4a shows an overlay of the initial velocity model on the seismic image. Figures 4b and 4c show the updates from the conventional and the new gradients respectively. The update from the conventional FWI is basically a mapping of the reflectivity or image into the velocity model, as I clear when compared to Figure 4a. When contrasted to the update from FWI with the new gradient, we can observe longer wavelength updates to the model to follow geology, but that do not constitute a simple mapping of reflectivity into the velocity field. To further evaluate the model derived from the new gradient, we performed Kirchhoff depth migration. We observed that the new FWI velocity model improved the flatness of the offset gathers as shown in Figures 4a and 4b.
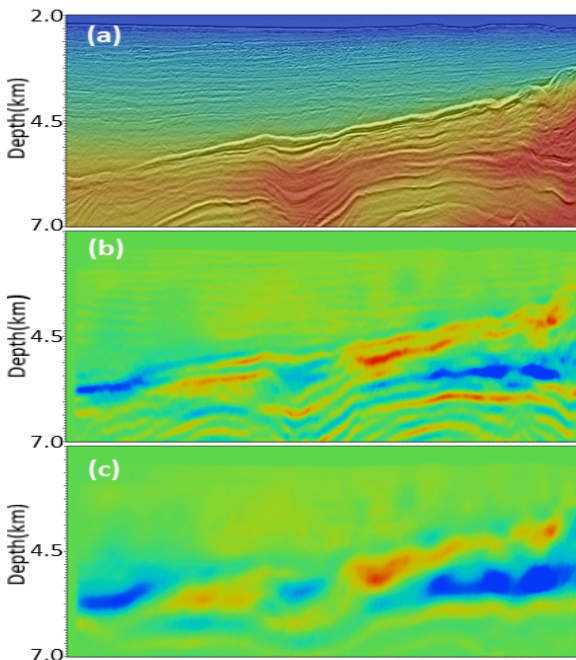

Figure 4. *2D dual sensor data example from deep water Gulf of Mexico: (a) initial velocity model overlaid by the seismic image, (b) conventional FWI model update, and (c) new FWI model update.*

As our second example, we show results for a wide-azimuth dual-sensor dataset acquired in deep water Gulf of Mexico (GOM) with maximum inline and crossline offsets of 7km and 4.2km, respectively. Here we deployed the new gradient combined with TV regularization. Figures 5a and 5b show depth slices (1440m and 1620m) of the initial velocity model computed from reflection tomography. We perform FWI from this model using a frequency bandwidth of 3-5 Hz. For the extrapolation of the wavefields, we use the pseudo-analytical method

assuming a TTI medium with variable density. Figures 5c and 5d show the corresponding slices for the inverted model. As observed, the new gradient allows updates to resolve small-scale lateral heterogeneities in the velocity model, provided mainly by the presence of diving waves. At the same time, there is no migration imprint in the updates produced by the specular reflections as observed in the vertical profiles for the starting and the inverted velocity models (Figures 6a and 6b).
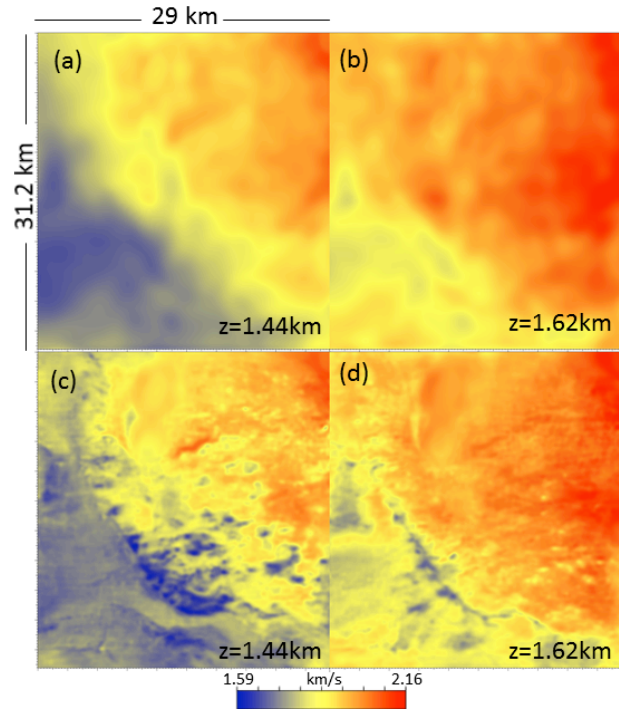

Figure 5. *Results for the wide-azimuth Gulf of Mexico dual-sensor data example new FWI gradient and TV regularization.*

Conclusions

We have described a new robust solution for recovering the long-wavelength features of a velocity model in gradient-based FWI. The method uses reflected and transmitted wave modes to recover high-resolution velocity models. The new FWI gradient enables reliable velocity updates deeper than the maximum penetration depth of diving waves, and reduces the FWI dependency on recording ultra-long offsets. Results from applying the new FWI gradient to field data show that we can combine both transmitted and reflected energy in a global FWI scheme to obtain high-resolution velocity models without imprint of the reflectivity on the velocity updates.

We have also shown a new FWI regularization scheme that can overcome the limitations of the inversion in the presence of high contrast geobodies and cycle skipping. The implementation makes use of the split Bregman method making it efficient and accurate. The numerical experiments demonstrate that our algorithm can deal with the challenges of the presence of high contrast geobodies and cycle skipping.
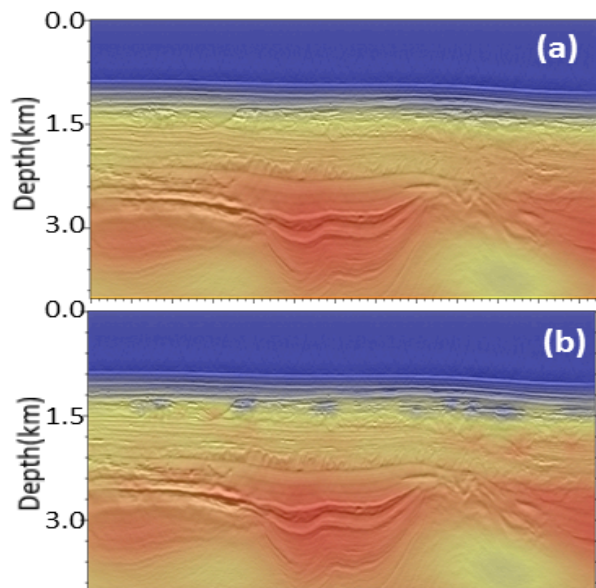
Figure 6. *Results for the wide-azimuth Gulf of Mexico dual-sensor data example using the dynamically weighted gradient: Vertical profiles for the (a) starting and the (b) inverted velocity model overlaid by the corresponding migrated stacked images. Horizontal distance is 18.6 km.*

Acknowledgments

References

Alkhalifah, T., 2014, Conditioning the full-waveform inversion gradient to welcome anisotropy, *Geophysics*, 80, R111-R122.

Liu, F., L. Guash, S.C. Morton, M. Warner, A. Umpleby, Z. Men, S. Fairhead and S. Chekles, 2012, 3D time-domain full waveform inversion of a Valhall OBC dataset, *82th Annual International Meeting, SEG*, Expanded Abstracts

Luo, Y., H. Zhu, T. Nissen-Meyer, C. Morency and J. Tromp, 2009, Seismic modeling and imaging based upon spectral-element and adjoint methods, *The Leading Edge*, 28, 569-574.

Tarantola, A.,1984, Inversion of seismic reflection data in the acoustic approximation, *Geophysics*, 49,1259-1266.

Whitmore, N.D. and S. Crawley, 2012, Application of RTM inverse scattering imaging conditions, 82nd Annual International Meeting*, SEG Expanded Abstracts*.

Xu, S., D. Wang, F. Chen, Y. Zhang, and G. Lambare, 2013, Full waveform inversion for reflected seismic data, *74th, EAGE Conference & Exhibition, Extended Abstracts.*

Zhou, W., R. Brossier, S. Operto and J. Vireux, 2015, Full waveform inversion of diving waves for velocity model building with impedance inversion based on scale separation, *Geophys. J. Int.*, 202, 1535-1554.

Zou, K., J. Ramos-Martínez, S. Kelly, A.A. Valenciano, N. Chemingui and J. Lie, 2014, Refraction Full-waveform Inversion in a Shallow Water Environment, *76th EAGE Conference & Exhibitio*n, Extended Abstracts.

Guitton, A. and Symes, W. W., 2003, Robust inversion of seismic data using the Huber norm. Geophysics, 68(4): 1310–1319, 2003.

Goldstein, T. and Osher, S., 2009, The split bregman method for l1- regularized problems. SIAM Journal on Imaging Sciences, 2(2):323–343.